Spin dephasing of Kr^{83}

C. H. Volk, J. G. Mark, and B. C. Grover
Litton Systems, Inc., Guidance and Control Systems Division, Woodland Hills, California 91365
(Received 22 June 1979)

The nuclear-spin dephasing of the noble gas Kr^{83} has been observed. A nonexponential decay signal, which is a function of the orientation of the experimental cell in the apparatus, has been measured. The spin decay characteristics of Kr^{83} have been explained in terms of an interaction of the nuclear quadrupole moment of Kr^{83} with the electric field gradients present at the nucleus during a collision of the Kr atom with the walls of the experimental cell. Qualitative agreement only is shown, since a complete quantitative analysis of the experiment is not available at the present time.

I. INTRODUCTION

The study of the spin dynamic characteristics of noble-gas nuclei in the presence of optically pumped alkali-metal vapors has been of interest since Bouchiat *et al.*[1] first polarized a gaseous He^3 ensemble in spin-exchange collisions with an optically oriented Rb vapor. We have been studying both the alkali-metal-atom–noble-gas-nucleus spin-exchange interaction and various aspects of nuclear gas spin relaxation using an alkali-metal vapor magnetometer technique developed by Cohen-Tannoudji *et al.*[2] In our typical experimental arrangement, we have a glass cell containing excess Rb metal, a buffer gas, usually N_2, in pressures from a few to several hundred Torr, which is present to facilitate the optical pumping of the Rb, and a noble gas in pressures of a few Torr. The Rb acts both to polarize the noble-gas nuclear ensemble through spin-exchange collisions and to detect the dynamic characteristic of the noble-gas nuclear polarization through the magnetometer mechanization. We have successfully employed this technique[3] to measure the spin-exchange cross section between Rb and Xe^{129}.

Recent measurements in our laboratory of the transverse decay rate of Kr^{83} showed that the decay of the nuclear polarization is dependent on the particular orientation of the NMR cell in the experimental apparatus. This effect was previously observed[4,5] in the relaxation of Hg^{201}. The particular orientation of the Hg^{201} cell which resulted in the longest T_2 decay time of the Hg polarization was termed the "magic angle," where the angle was between the cell axis and the externally applied magnetic field.[4] No such angular effects have been observed in either Xe^{129} or Hg^{199}, both of which have nuclear spin $I=\frac{1}{2}$. This suggests that the angular effect results from quadrupolar-type interactions present in Kr^{83} and Hg^{201} decay. In this report we will consider possible relaxation phenomena associated with quadrupolar interactions present in nuclei with spin greater than $\frac{1}{2}$, developing particular expressions for nuclear spin species $I=\frac{9}{2}$, Kr^{83}, and $I=\frac{3}{2}$, Xe^{131} and Hg^{201}.

II. EXPERIMENTAL OBSERVATIONS

Typical precessional decay data for a Kr^{83} sample is displayed in Figs. 1 and 2. Our experimental technique for measuring noble gas relaxation times has been described previously,[3] and will not be reviewed here. This particular sample contained natural Rb metal, 150-Torr N_2 and 5-Torr Kr^{83} in a 1-ml Corning 1720 glass cell. Figs. 1 and 2 represent data taken at the same temperature, approximately 60 °C, after an initial constant pump time with each plot corresponding to a different orientation of the cell in the experimental apparatus. The data stream in each plot is 500 sec long. The angle indicated on each plot is taken between the cell axis and the externally applied magnetic field. The cell axis was taken to be along a line that passes symmetrically through the tip-off region of the cell as a matter of convenvenience.

A. General features of the data

We enumerate general observations concerning data (i) T_2 decay of the Kr^{83} spin system is a function of angular orientation of the cell in the experimental apparatus. (ii) The Kr signals cannot be soley described by an exponential decay. In addition, the nonexponential character of the decay is a function of angle. (iii) The precession frequency is a function of time and cell orientation. This can be seen by comparing Figs. 1(a) and 1(b). Also, comparing Figs. 1(a) and 1(c), one sees an indication of a possible phase reversal in the second cycle of Fig. 1(c). (iv) The decay characteristics at a particular angle designation are a function of the position of the Rb metal reservoir in the cell. In the sample shown, the magic angle for the cell was at or near 92 °. The magic angle for the cell

 © 1979 The American Physical Society

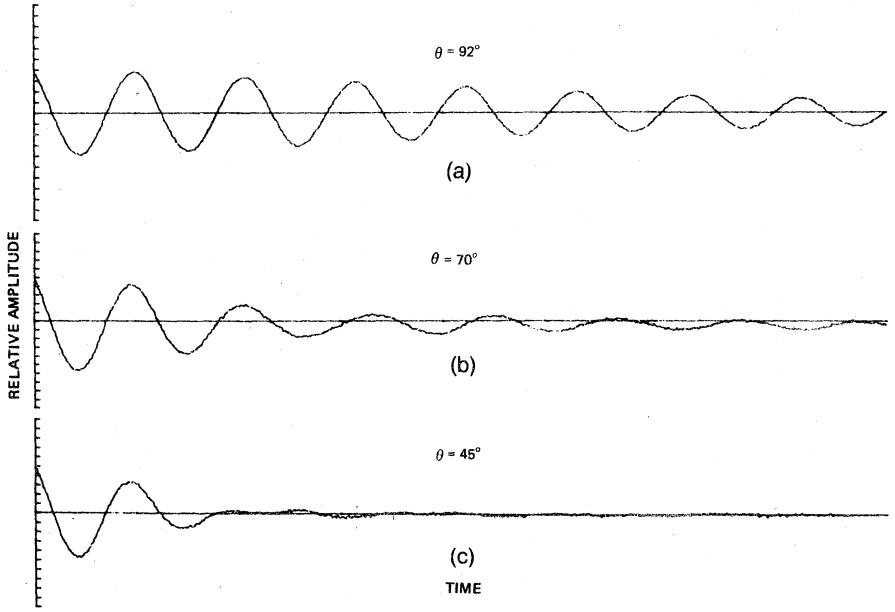

FIG. 1. Precessional decay data for Kr^{83}.

can therefore be changed by moving the Rb distribution on the cell walls. (v) Previous measurements of the Kr decay characteristics as a function of cell size demonstrated a significant contribution to the relaxation processes from wall effects. (vi) The initial amplitudes appear to be constant as a function of angle, implying that the angular effect does not significantly contribute to the T_1 process of the Kr spin system.

III. TRANSVERSE RELAXATION EFFECTS

Transverse (i.e., T_2) relaxation refers to the loss of phase coherence in a precessing spin system. Spin dephasing in a quadrupolar interaction can arise through both an inhomogeneous broadening of the nuclear Zeeman levels and trans-transitions among the energy levels.[6]

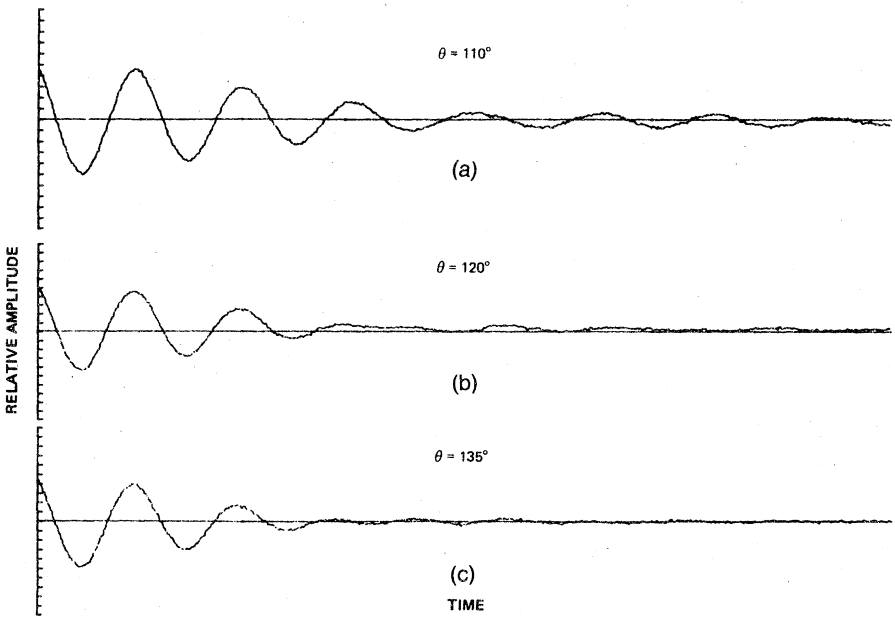

FIG. 2. Precessional decay data for Kr^{83}.

A. Level shifts due to a quadrupolar interaction

We take the full spin Hamiltonian to be

$$H = H_M + H_Q, \tag{1}$$

where H_M is the static magnetic interaction

$$H_M = -\gamma h H_0 I_z \tag{2}$$

with γ the nuclear gyromagnetic ratio, H_0 the external magnetic field, taken to be along the z axis, and I_z the z component of nuclear spin. H_Q, the quadrupole Hamiltonian, represents the interaction of the nuclear quadrupole moment with electric field gradients. It can be written[7,8]:

$$H_Q = \frac{eQ}{6I(2I-1)} \sum_{j,k} \frac{\partial^2 V}{\partial x_j \partial x_k} \times \left[\tfrac{3}{2}(I_j I_k + I_k I_j) - \delta_{jk} I(I+1)\right]. \tag{3}$$

The indices j and k refer to axes x, y, and z. Q is the quadrupole moment of the nucleus, e is the elemental charge, $\partial^2 V/\partial x_j \partial x_k$ represents a component of the electric field gradient tensor. To simplify the calculation, we limit ourselves to electric field gradients with cylindrical symmetry and designate $eq = \partial^2 V/\partial z'^2$, where z' is then the cylindrical axis of the field gradient. The quadrupole Hamiltonian becomes

$$H_Q = \frac{e^2 Qq}{4I(2I-1)} \left\{\tfrac{1}{2}(3\cos^2\theta - 1)[3I_z^2 - I(I+1)] + \tfrac{3}{2}\sin\theta\cos\theta[I_z(I^+ + I^-) + (I^+ + I^-)I_z] + \tfrac{3}{4}\sin^2\theta(I^{+2} + I^{-2})\right\}, \tag{4}$$

where θ is the angle between the z and z' axes, and $I^\pm$ are the raising and lowering operators associated with the spin operator I, in the Cartesian reference[9]:

$$I^\pm = I_x \pm i I_y. \tag{5}$$

With the following definitions:

$$a = (3\cos^2\theta - 1), \tag{6a}$$

$$b = \sin\theta\cos\theta, \tag{6b}$$

$$c = \sin^2\theta, \tag{6c}$$

$$\alpha = e^2 Qq/4I(2I-1), \tag{6d}$$

$$\omega = -\gamma H_0, \tag{6e}$$

the Hamiltonian matrices for the spin systems $I = \frac{3}{2}$ and $I = \frac{9}{2}$ are as shown in Figs. 3 and 4 respectively.

The energy levels of the system are found through second-order perturbation theory[10]:

$$H = \begin{bmatrix} \frac{3}{2}\omega + \frac{3}{2}\alpha a & 3\sqrt{3}\,\alpha b & \frac{3\sqrt{3}}{2}\alpha c & 0 \\ 3\sqrt{3}\,\alpha b & \frac{1}{2}\omega - \frac{3}{2}\alpha a & 0 & \frac{3\sqrt{3}}{2}\alpha c \\ \frac{3\sqrt{3}}{2}\alpha c & 0 & -\frac{1}{2}\omega - \frac{3}{2}\alpha a & -3\sqrt{3}\,\alpha b \\ 0 & \frac{3\sqrt{3}}{2}\alpha c & -3\sqrt{3}\,\alpha b & -\frac{3}{2}\omega + \frac{3}{2}\alpha b \end{bmatrix}$$

FIG. 3. Hamiltonian matrix for spin system $I = \frac{3}{2}$.

$$H = \begin{bmatrix} \frac{9}{2}\omega + 18\,\alpha a & 36\,\alpha b & 9\,\alpha c & 0 & 0 & 0 & 0 & 0 & 0 & 0 \\ 36\,\alpha b & \frac{7}{2}\omega + 6\,\alpha a & 36\,\alpha b & 3\sqrt{21}\,\alpha c & 0 & 0 & 0 & 0 & 0 & 0 \\ 9\,\alpha c & 36\,\alpha b & \frac{5}{2}\omega - 3\,\alpha a & 6\sqrt{21}\,\alpha b & \frac{9}{2}\sqrt{14}\,\alpha c & 0 & 0 & 0 & 0 & 0 \\ 0 & 3\sqrt{21}\,\alpha c & 6\sqrt{21}\,\alpha b & \frac{3}{2}\omega - 9\,\alpha a & 6\sqrt{6}\,\alpha b & \frac{15}{2}\sqrt{6}\,\alpha c & 0 & 0 & 0 & 0 \\ 0 & 0 & \frac{9}{2}\sqrt{14}\,\alpha c & 6\sqrt{6}\,\alpha b & \frac{1}{2}\omega - 12\,\alpha a & 0 & \frac{15}{2}\sqrt{6}\,\alpha c & 0 & 0 & 0 \\ 0 & 0 & 0 & \frac{15}{2}\sqrt{6}\,\alpha c & 0 & -\frac{1}{2}\omega - 12\,\alpha a & -6\sqrt{6}\,\alpha b & \frac{9}{2}\sqrt{14}\,\alpha c & 0 & 0 \\ 0 & 0 & 0 & 0 & \frac{15}{2}\sqrt{6}\,\alpha c & -6\sqrt{6}\,\alpha b & -\frac{3}{2}\omega - 9\,\alpha a & -6\sqrt{21}\,\alpha b & 3\sqrt{21}\,\alpha c & 0 \\ 0 & 0 & 0 & 0 & 0 & \frac{9}{2}\sqrt{14}\,\alpha c & -6\sqrt{21}\,\alpha b & -\frac{5}{2}\omega - 3\,\alpha a & -36\,\alpha b & 9\,\alpha c \\ 0 & 0 & 0 & 0 & 0 & 0 & 3\sqrt{21}\,\alpha c & -36\,\alpha b & -\frac{7}{2}\omega + 6\,\alpha a & -36\,\alpha b \\ 0 & 0 & 0 & 0 & 0 & 0 & 0 & 9\,\alpha c & -36\,\alpha b & -\frac{9}{2}\omega + 18\,\alpha a \end{bmatrix}$$

FIG. 4. Hamiltonian matrix for spin system $I = \frac{9}{2}$.

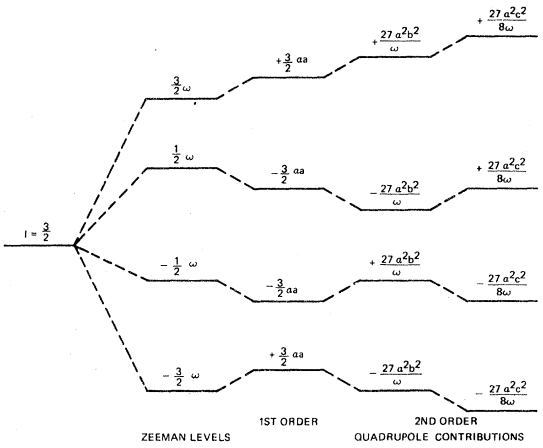

FIG. 5. Energy-level diagram for spin system $I=\frac{3}{2}$, with energy levels defined by Eq. (7) under the Hamiltonian defined in Eq. (1) with terms defined in Eqs. (6a)–(6e).

$$E_m^{(2)}=E_m^o+\langle m|H|m\rangle+\sum_j \frac{|\langle m|H|j\rangle|^2}{E_m^o-E_j^o}, \tag{7}$$

where we have taken the quadrupole interaction as a perturbation of the Zeeman term. From Eq. (7), with the aid of Figs. 3 and 4, we can construct an energy-level diagram, as shown in Figs. 5 and 6 for the spin systems $I=\frac{3}{2}$ and $I=\frac{9}{2}$, respectively.

B. Effects of energy-level shifts on the precessing spin system

We experimentally observe the spin dephasing of a precessing nuclear sample by first creating a longitudinal nuclear polarization through spin exchange with optically pumped alkali-metal vapor and then rotating the external magnetic field by 90° to initiate precession of the nuclear spins. We equivalently describe this process in terms of the noble-gas density matrix. We restrict ourselves here to nuclear spin $I=\frac{3}{2}$; however, analogous equations can be written for the spin $I=\frac{9}{2}$ case.

We assume that as a result of the alkali-metal–noble-gas spin-exchange interaction, the noble-gas nucleus attains some low degree of polarization. In the low polarization limit, the density matrix for the noble-gas system can be written[11]:

$$\rho=\begin{pmatrix} \frac{1}{4}+\frac{3}{2}\zeta & 0 & 0 & 0 \\ 0 & \frac{1}{4}+\frac{1}{2}\zeta & 0 & 0 \\ 0 & 0 & \frac{1}{4}-\frac{1}{2}\zeta & 0 \\ 0 & 0 & 0 & \frac{1}{4}-\frac{3}{2}\zeta \end{pmatrix}, \tag{8}$$

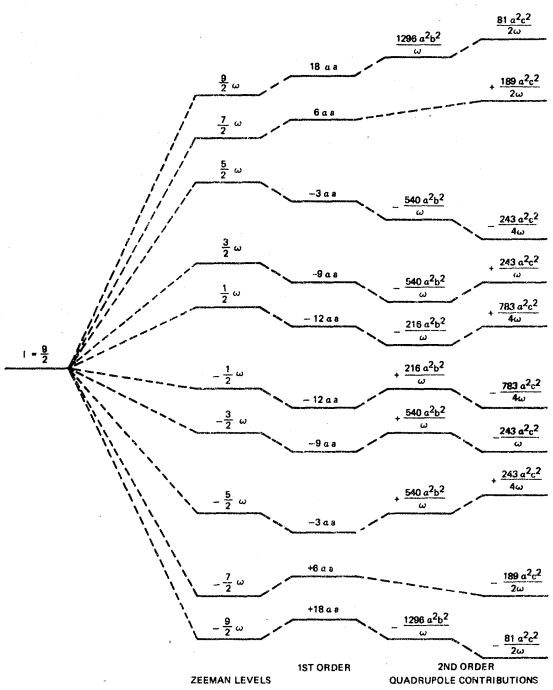

FIG. 6. Energy-level diagram for spin system $I=\frac{9}{2}$, with energy levels defined as in Fig. 5.

where ζ is a small number compared to unity. The factor $\frac{1}{4}$ is the equilibrium population density of each level. We can rewrite the initially prepared density matrix:

$$\rho=\tfrac{1}{4}[I]+\zeta\begin{pmatrix} \frac{3}{2} & 0 & 0 & 0 \\ 0 & \frac{1}{2} & 0 & 0 \\ 0 & 0 & -\frac{1}{2} & 0 \\ 0 & 0 & 0 & -\frac{3}{2} \end{pmatrix}, \tag{9}$$

where $[I]$ is the identity matrix.

Rotating the magnetic fields in the experimental apparatus is equivalent to a rotation of the density matrix, which is given by:

$$\rho'=D\rho D^t, \tag{10}$$

where D is a Wigner D matrix.[12] The D matrix for a rotation of a spin-$\frac{3}{2}$ system about the y axis through an angle ρ is shown in Fig. 7. Substituting Eq. (9) into Eq. (10) and using Fig. 7, we find the initial state of the rotated density matrix:

$$\rho'(0)=\tfrac{1}{4}[I]+\zeta\begin{pmatrix} \cos\beta & -\sqrt{3}\sin\beta & 0 & 0 \\ -\sqrt{3}\sin\beta & \cos\beta & -2\sin\beta & 0 \\ 0 & -2\cos\beta & -2\cos\beta & -\sqrt{3}\sin\beta \\ 0 & 0 & 0 & -\cos\beta \end{pmatrix}. \tag{11}$$

$$D^{3/2}(0,\beta,0) = \begin{bmatrix} \cos^3\beta/2 & \sqrt{3}\cos^2\beta/2\sin\beta/2 & \sqrt{3}\cos\beta/2\sin^2\beta/2 & \sin^3\beta/2 \\ -\sqrt{3}\cos^2\beta/2\sin\beta/2 & \cos^3\beta/2 - 2\cos\beta/2\sin^2\beta/2 & -\sin^3\beta/2 + 2\cos^2\beta/2\sin\beta/2 & \sqrt{3}\cos\beta/2\sin^2\beta/2 \\ \sqrt{3}\cos\beta/2\sin^2\beta/2 & \sin^3\beta/2 - 2\cos^2\beta/2\sin\beta/2 & \cos^3\beta/2 - 2\cos\beta/2\sin^2\beta/2 & \sqrt{3}\cos^2\beta/2\sin\beta/2 \\ -\sin^3\beta/2 & \sqrt{3}\cos\beta/2\sin^2\beta/2 & -\sqrt{3}\cos^2\beta/2\sin\beta/? & \cos^3\beta/2 \end{bmatrix}$$

FIG. 7. D matrix for a rotation of a spin-$\frac{3}{2}$ system about the y axis through an angle β.

The precessional characteristics of the spin sample are described by the time evolution of the density matrix. The time dependence of the density matrix is given by:

$$\rho'(t) = U(t,0)\rho'(0)U^t(t,0), \tag{12}$$

where the evolution operator, $U(t,0)$ is defined through the differential equation:

$$\dot{U}(t,0) = -iU(t,0)H \tag{13}$$

with the condition

$$U(0,0) = [I]. \tag{14}$$

In solving Eq. (13), we have assumed that the quadrupolar contribution is small so that we may maintain the original eigenvectors of the magnetic Hamiltonian while taking the eigenvalues through second-order perturbation. The evolution operator becomes:

$$U(t,0) = \begin{bmatrix} \exp(-iE_{3/2}t) & 0 & 0 & 0 \\ 0 & \exp(-iE_{1/2}t) & 0 & 0 \\ 0 & 0 & \exp(-iE_{-1/2}t) & 0 \\ 0 & 0 & 0 & \exp(-iE_{-3/2}t) \end{bmatrix}. \tag{15}$$

The time dependence of the density matrix, using Eqs. (11), (12) and (15), is displayed in Fig. 8.

The signal observed in our experiments corresponds to the expectation value of the x component of the noble-gas polarization, $\langle I_x\rangle$, defined to be:

$$\langle I_x\rangle = \mathrm{Tr}[I_x\rho'] \tag{16}$$

with the operator I_x for the spin-$\frac{3}{2}$ system written in matrix form as:

$$I_x = \tfrac{1}{2}\begin{bmatrix} 0 & \sqrt{3} & 0 & 0 \\ \sqrt{3} & 0 & 0 & 0 \\ 0 & 0 & 0 & \sqrt{3} \\ 0 & 0 & \sqrt{3} & 0 \end{bmatrix}. \tag{17}$$

Thus our experiment is found to correspond to the following equation:

$$\langle I_x\rangle(t) = -\tfrac{1}{2}\zeta\sin\beta[3\cos(E_{3/2}-E_{1/2})t + 4\cos(E_{1/2}-E_{-1/2})t + 3\cos(E_{-1/2}-E_{-3/2})t]. \tag{18}$$

For the case in which the quadrupole interaction is not present, the energy differences all become the same and Eq. (18) collapses to:

$$\langle I_x\rangle(t) = -5\zeta\sin\beta\cos\omega t, \tag{19}$$

which simply describes the free precession of the spin system in a magnetic field. Writing out the frequency terms in Eq. (18) we have:

$$E_{3/2} - E_{1/2} = \omega + 3\alpha a + 54\alpha^2 b^2/\omega, \tag{20a}$$

$$E_{1/2} - E_{-1/2} = \omega - 54\alpha^2 b^2/\omega + 27\alpha^2 c^2/4\omega, \tag{20b}$$

$$E_{-1/2} - E_{-3/2} = \omega - 3\alpha a + 54\alpha^2 b^2/\omega, \tag{20c}$$

noting that the terms a, b, and c have angular dependence. From Eq. (18), we see that a quadrupole-type interaction results in three precession frequencies for a spin-$\frac{3}{2}$ system. In general then, a spin system described by spin I will have 2I precession frequencies in the presence of a quadrupole-type interaction. The different frequencies can be seen to be not only a function of the strength of the quadrupole interaction but also of the relative orientation of the electric field gradient with respect to the external magnetic field direction.

Examples of the precession signal described by Eq. (18) are displayed in Fig. 9. Figure 9a is an example of the free precession signal in the absence of any quadrupole interaction, presented for

$$\rho'(t) = \begin{bmatrix} \cos\beta & -\sqrt{3}\sin\beta\, e^{-i(E_{3/2}-E_{1/2})t} & 0 & 0 \\ -\sqrt{3}\sin\beta\, e^{i(E_{3/2}-E_{1/2})t} & \cos\beta & -2\sin\beta\, e^{-i(E_{1/2}-E_{-1/2})t} & 0 \\ 0 & -2\sin\beta\, e^{i(E_{1/2}-E_{-1/2})t} & -\cos\beta & -\sqrt{3}\sin\beta\, e^{-i(E_{-1/2}-E_{-3/2})t} \\ 0 & 0 & -\sqrt{3}\sin\beta\, e^{i(E_{-1/2}-E_{-3/2})t} & -\cos\beta \end{bmatrix}$$

FIG. 8. Density-matrix time dependence.

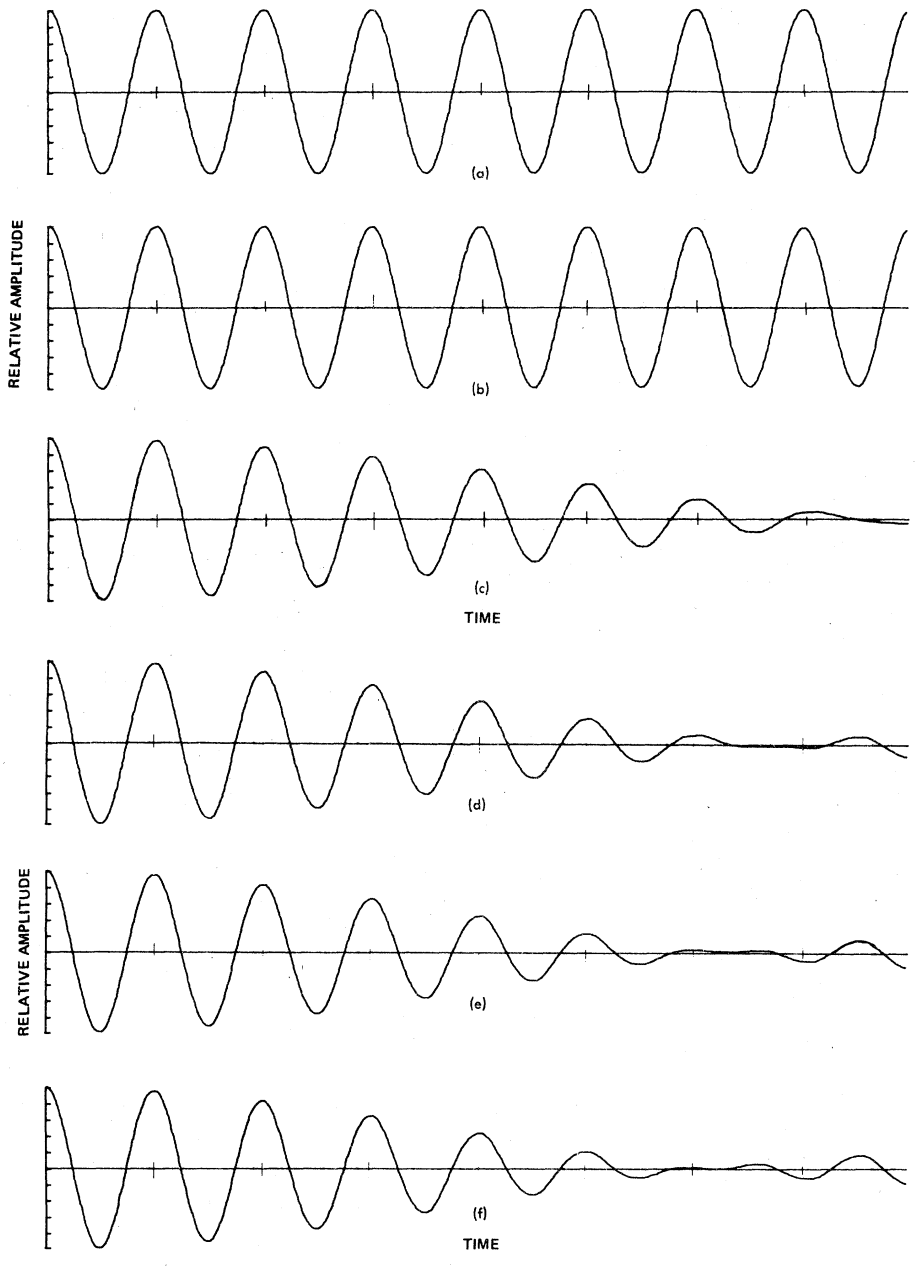

FIG. 9. Free precession signal without quadrupolar interaction (a), with quadrupolar-interaction curves for $\theta = 55°$ (b), 75° (c), 80° (d), 85° (e), and 90° (f) given for comparison.

the purpose of comparing the effects of the presence of the quadrupolar interaction. The strength of the quadrupole interaction is the same in Figures 9(b)–9(f) and was taken to be 2% of the magnetic interaction, based on estimates from the experimental data. The plot displays the effect of the angular orientation.

Figure 9(b) was attained by forcing the first-order contribution of the quadrupolar interaction to zero. This is accomplished by setting the term $(3\cos^2\theta-1)$ to zero. The angle θ is found to be approximately 55°, which has previously been designated as the magic angle.[4] Figure 9(c) corresponds to an angular orientation of 75°, about 20° off the magic angle; Figs. 9(d), 9(e), and 9(f) represent orientations of 80, 85, and 90°, respectively. The tick marks on all the plots designate the time position of the positive peaks of the free magnetic precession signal.

Various aspects of the Kr^{83} data can now be explained in terms of our model, albeit the model was derived from a spin-$\frac{3}{2}$ system.

(a) There is an apparent decay of the precession signal as a function of angle. It is apparent in the sense that Eq. (18) describes three oscillatory signals which beat with one another. The beat envelope then is interpreted as a decay. If we were to extend the time axis on Figs. 9(c)–9(f), one would see the signal increase again in time. This phenomenon is not seen in the actual Kr data due to the presence of other decay processes which drive the signal amplitude to zero.

(b) The beat envelope is not an exponential function. The Kr data is some combination of exponential decay due to "real" decay processes modulated by the beat frequency. Near the magic angle, the signal is well described by an exponential function and quadrupolar effects are at a minimum, at angles more distant from the magic angle, the decay signal develops a more nonexponential character.

(c) Using the tick marks on the plots as a reference one can see that the precession frequency becomes shorter with time as a function of angle Figures 9(d)–9(f) show a phase reversal in the decay signal.

C. Origin of the angular effects

We noted earlier that the Kr decay data was influenced by the position of the excess Rb metal on the walls of the cell and that the Kr spin-relaxation rate was a function of the cell size. We understand these facts to imply that the Kr experiences a quadrupole interaction in collisions with the cell walls. It has been suggested that in a collision of a noble-gas atom with a cell wall, the atom is temporarily bound to the wall through a Van der Waals type interaction.[6] The depth of the well between the atom and a particular wall site is proportional to the surface adhesion energy. The electronic charge cloud of the atom undergoes a distortion during the atom-wall interaction which results in an electric field gradient at the nucleus, proportional to the curvature of the potential well.

Within this model, we can divide the binding sites on the cell walls into two distinct classes: one in which the noble-gas atoms bind directly to the glass wall and the other in which the noble-gas atoms bind to the layer of deposited Rb metal. One would expect that the adhesion energies between noble-gas atoms and glass to be different from those of noble-gas atoms and alkali metal. Since it is observed that the alkali metal does not uniformly distribute over the glass surface, then it must be true that there is an angular distribution of adhesion sites on the cell wall. Note that this argument does not depend on the strength of the binding energy of the noble-gas-atom–glass sites compared to the noble-gas-atom–alkali-metal sites; it requires only that the adhesion be different between the two classes of sites. In addition, the angular distribution of binding sites will be only weakly dependent on the macroscopic shape of the cell. The angular dependence in the Kr data results from the averaging over the binding sites with respect to the z axis defined by the external magnetic field; as the cell is rotated, the averaging with respect to the space stationary z axis changes and yields the observed angular effect. Redistributing the excess Rb metal on the cell wall changes the angular distribution of the binding sites and thus changes the angular effect at a particular cell orientation. Wall collision effects on spin systems exhibit a strong dependence on the surface-to-volume ratio of the cell. This general feature has been observed in our experiments, which gives us confidence in our model of the Kr wall collisions.

D. Level transition effects

The true relaxation rate of a spin system through a quadrupole coupling of the nucleus with the electric field gradients which appear at the nucleus during the interaction of an atom on a wall has been worked out for Hg^{201} by Cohen-Tannoudji.[8] The time evolution of the nuclear density matrix is given by the formula:

$$\frac{d\rho}{dt} = -\int_0^\infty (H_Q^*(t), [H_Q(t-\tau), \rho(t)])_{av}\, d\tau\,, \qquad (21)$$

which is second order in the quadrupole Hamiltonian as compared to the pseudorelaxation through level shifting which is first order in the interaction

Hamiltonian.

Equation (21) also governs the longitudinal effects due to the quadrupole interaction. The degree of angular effect resulting from relaxation described by Eq. (21) would be readily apparent in the measured T_1 rate; however, no angular effects have been observed in the Kr T_1 measurements and thus we conclude that we may average over all angles uniformly in the solution of Eq. (21) and directly apply Cohen-Tannoudji's results to the spin-$\frac{3}{2}$ system.

The fact that level transitions do not yield angular effects in the relaxation rates while the inhomogeneous line broadening results in a significant angular dependence can be understood in the following way. Spin dephasing due to the energy-level shifts is proportional to the interaction Hamiltonian while relaxation through level transitions is proportional to the square of the interaction Hamiltonian. We have estimated the average strength of the quadrupole interaction in our Kr^{83} experiments to be about 2% of the Zeeman interaction strength. This implies that the energy-level transition rate due to the quadrupole interaction is about two orders of magnitude smaller that the dephasing rate due to line broadening. Thus, orientation effects from level transitions would be very much depressed and negligible in our work.

For isotropic orientations of the electric field gradient, Eq. (21) is shown to become

$$\frac{d\rho}{dt} = -\tfrac{1}{36}\sum_r J_r(A^r,[A^{-r},\rho(t)]), \tag{22}$$

where the index r runs from -2 to $+2$ and

$$A^0 = 3I_z^2 - I(I+1), \tag{23a}$$

$$A^{\pm 1} = \sqrt{\tfrac{6}{2}}(I_z I^{\pm} + I^{\pm} I_z), \tag{23b}$$

$$A^{\pm 2} = \sqrt{\tfrac{6}{2}}(I^{\pm})^2, \tag{23c}$$

$$J_r = J_{-r} = \frac{36\pi}{5}\frac{\tau_s}{\tau_s+\tau_v}\left(\frac{e^2qQ}{I(2I-1)}\right)^2 \frac{\tau_c}{1+(r\omega\tau_c)^2}. \tag{24}$$

For the magnetic fields present in our experiments, $(r\omega\tau_c)^2 \ll 1$ and thus the quadrupole relaxation described by Eq. (21) is characterized by a single rate constant J in our experiments. From Eq. (13b) of Ref. 7, the decay of the transverse polarization can be shown to be given by the following formula:

$$\langle \dot{I}_x \rangle = -2J\langle I_x \rangle, \tag{25}$$

which is a simple exponential decay function. The complete transverse decay of a spin system due to a quadrupole interaction is described by the function represented in Eq. (18) multiplied by the above exponential decay.

IV. SUMMARY

We measured the transverse nuclear decay characteristics of Kr^{83} and found that the decay is strongly dependent upon the orientation of the experimental cell in the externally applied magnetic fields in the apparatus. The general features of the Kr^{83} spin decay have been explained in terms of an inhomogeneous broadening of the nuclear Zeeman levels due to the interaction of the nuclear quadrupole moment with electric field gradients present at the nucleus. A quantitative analysis of the Kr^{83} data is not available at the present time due to the complexity of the Kr nuclear levels. We plan to continue this work using Xe^{131} in order to make a more quantitative study of this phenomenon.

ACKNOWLEDGMENTS

We wish to acknowledge the invaluable assistance of Roger L. Meyer in the preparation of the apparatus used in this work. The research was supported in part by the Air Force Office of Scientific Research under Contract NO. F49620-77-C-0047.

[1] M. A. Bouchiat, T. R. Carver, and C. M. Varnum, Phys. Rev. Lett. 5, 373 (1960).
[2] C. Cohen-Tannoudji, J. Dupont-Roc, S. Haroche, and F. Laloe, Rev. Phys. Appl. 5, 95 (1970).
[3] B. C. Grover, Phys. Rev. Lett. 40, 391 (1978).
[4] D. S. Bayley, I. A. Greenwood, and J. H. Simpson, Noise Sources in NMR Oscillators and Relaxation Phenomena in Optically Pumped Mercury Isotopes, Final Scientific Report, AFOSR, 1976 (unpublished).
[5] J. H. Simpson, Bull. Am. Phys. Soc. 23, 394 (1978).
[6] W. Happer (private communication).
[7] A. Abragam, *The Principle of Nuclear Magnetism* (Clarendon, Oxford, 1961), Chap. 8.
[8] C. Cohen-Tannoudji, J. Phys. (Paris) 24, 653 (1963).
[9] L. I. Schiff, *Quantum Mechanics* (McGraw-Hill, New York, 1968), p. 200.
[10] L. I. Schiff, in Ref. 9, p. 247.
[11] L. W. Anderson and A. T. Ramsey, Phys. Rev. 124, 1862 (1961).
[12] A. R. Edmonds, *Angular Momentum in Quantum Mechanics*, (Princeton University, Princeton, N. J., 1957), Chap. 4.